Vol 12 No 11, November 2003
1009-1963/2003/12(11)/1272-11

Chinese Physics

© 2003 Chin. Phys. Soc.
and IOP Publishing Ltd

Microstructural evolution during containerless rapid solidification of Co-Si alloys*

Yao Wen-Jing(姚文静) and Wei Bing-Bo(魏炳波)

Laboratory of Materials Science in Space, Department of Applied Physics, Northwestern Polytechnical University, Xi'an 710072, China

(Received 11 April 2003; revised manuscript received 27 May 2003)

The Co-12%Si hypoeutectic, Co-12.52%Si eutectic and Co-13%Si hypereutectic alloys are rapidly solidified in a containerless environment in a drop tube. Undercoolings up to 207K ($0.14T_{\rm E}$) are obtained, which play a dominant role in dendritic and eutectic growth. The coupled zone around Co-12.52%Si eutectic alloy has been calculated, which covers a composition range from 11.6 to 12.7%Si. A microstructural transition from lamellar eutectic to divorced eutectic occurs to Co-12.52%Si eutectic droplets with increasing undercooling. The lamellar eutectic structure of the Co-12.52%Si alloy consists of εCo and Co_3Si phases at small undercooling. The Co_3Si phase cannot decompose completely into εCo and αCo_2Si phases. As undercooling becomes larger, the Co_3Si phase grows very rapidly from the highly undercooled alloy melt to form a divorced eutectic. The structural morphology of the Co-12%Si alloy droplets transforms from εCo primary phase plus lamellar eutectic to anomalous eutectic, whereas the microstructure of Co-13%Si alloy droplets experiences a 'dendritic to equiaxed' structural transition. No matter how large the undercooling is, the εCo solid solution is the primary nucleation phase. In the highly undercooled alloy melts, the growth of εCo and Co_3Si phases is controlled by solutal diffusion.

Keywords: rapid solidification, containerless processing, Co-Si alloy, eutectic growth
PACC: 6125M, 6150J, 6155H, 6470D

1. Introduction

Extensive research about Co-based alloy systems has been accomplished not only in materials science but also in condensed matter physics. The investigations into these alloy systems have achieved many significant results. For example, Co-Cu alloys attract great research interest for their unique magnetic properties and many potential applications.[1,2] Information concerning the structural disorder and thermochemistry in the Co-Ti system is essential for the development of magnetic and optical materials of Co-based superalloys. The influence of structural disorder on the magnetic, optical and transport properties of Co-Ti alloy films are investigated by Lee *et al.*[3] For Co-Pd binary alloys, the atomic structure anisotropy between Co-Pd alloys and Co/Pd multilayer films is compared. Kim *et al*[4] employed Co K-edge extended x-ray absorption fine structure measurements with linear polarization dependence to investigate the chemical short-range order and interatomic distance anisotropy in Co-Pd alloys and Co/Pd multilayer films. The Co-Si binary alloy system is fascinating, because it involves a $CoSi_2$ intermetallic compound, which is an important electronic material. Based on the equilibrium phase diagram of Co-Si alloys, as evaluated by Ishida and Nishizawa,[5] there exist four eutectic transformations, which involve more than four intermetallic compounds. So far, research work on Co-Si alloys has been focused on the structures and properties of these alloys with high silicon content.[6–8] $CoSi_2$ compound is regarded as a good choice for deep submicrometre device fabrication since it has several important advantages, such as no linewidth effect on the sheet resistivity and no strong interaction with the dopants. On the basis of the previous study about the rapid solidification of Co-Si alloys with high silicon content,[9] the Co-Si alloys with low silicon content are investigated.

To observe the microstructural evolution of low-

*Project supported by the National Natural Science Foundation of China (Grant Nos 50221101, 50291015 and 50271058), Fok Ying-Tong Education Foundation, China (Grant No 71044) and Doctorate Foundation of Northwestern Polytechnical University, China (Grant No 200243).

silicon-content Co-Si alloys, drop tube technique is used to realize the rapid solidification under containerless state. Free fall method is an essential way to simulate the containerless state and reduced gravity on ground instead of the expensive experiments in outer space. Drop tube, which can not only disperse the sample into many small liquid droplets to obtain containerless state but also produce reduced gravity, is a kind of experimental equipment using free fall technique.[10−16] Containerless state can be used to avoid the touch of alloy melt with container wall to eliminate the heterogeneous nuclei and obtain high undercoolings. In order to reduce the influence of gravity on the solidification microstructures within containerless state, drop tube may be a preferable choice to study the kinetics of rapid solidification.

The investigation of Co-12.52%Si eutectic alloy is helpful to understand the competitive nucleation and the cooperative growth of metal solid solution and compound phase. Meanwhile, the investigations for the off-eutectic alloys can make clear about the competitive nucleation and growth of primary phases during the nonequilibrium solidification. The purpose of this work is to provide a deep insight into the microstructural transitions, occurring to Co-12%Si hypoeutectic, Co-12.52%Si eutectic and Co-13%Si hypereutectic alloys under containerless state. Furthermore, their rapid solidification mechanisms are analysed by LKT/BCT dendritic growth and TMK eutectic growth theories.

2. Experimental procedure

The experiments were performed in a 3 m drop tube. The master alloy was prepared by induction melting from pure Co (99.95%) and pure Si (99.99%), and each sample had a mass of about 0.5g. When an experiment began, the sample was placed in a 13 mm $ID \times 15$mm $OD \times 160$mm quartz tube, the bottom of which had a small orifice about 0.2 mm in diameter. The quartz tube was then installed on the top of the drop tube. Afterwards the drop tube was evacuated to 5.0×10^{-5}Pa before backfilled with a mixture of He and Ar gas to about 0.1MPa. The sample was melted by induction heating and further overheated to about 100K above its liquidus temperature for several minutes. The temperature was measured by an infrared pyrometer, and then the melt was ejected out from the orifice and dispersed into many fine droplets after being blown by a gas flow of highly purified He or Ar into the quartz tube. The solidified droplets were collected at the bottom of the drop tube and sieved into several groups according to their sizes. The solidified particles were mounted in epoxy, sectioned, polished, and, etched with a mixture of 30ml hydrofluoric acid +10ml HNO_3 +10ml H_2O. The microstructures of the solidified particles were analysed by XJG-05 optical microscope and Armary B1000 and S2700 scanning electron microscope (SEM). The phase composition was identified by energy dispersive spectroscopy (EDS). x-ray diffraction (XRD) is used to distinguish Co_3Si phase from αCo_2Si phase.

3. Results and discussion

The locations of Co-12%Si hypoeutectic, Co-12.52%Si eutectic and Co-13%Si hypereutectic alloys are illustrated in the phase diagram together with the calculated eutectic coupled zone, as shown in Fig. 1. It can be seen that under equilibrium conditions, Co-12.52%Si eutectic alloy is composed of 29.8vol.% εCo solid solution and 70.2vol.% Co_3Si intermetallic compound. The Co-12%Si hypoeutectic microstructure consists of 48.6vol.% primary εCo phase plus 51.4vol.% eutectic microstructure, whereas Co-13%Si hypereutectic alloy contains 79.9vol.% primary Co_3Si phase plus 20.1vol.% eutectic microstructure. It is worthy of notice that there is a eutectoid transformation below the eutectic line. In other words, the solidified Co_3Si compound will decompose into 48.7vol.%

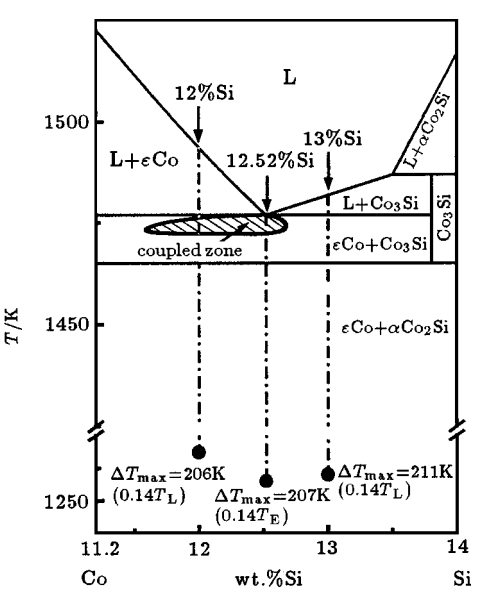


Fig.1. Maximum undercoolings and calculated eutectic coupled zone shown in Co-Si binary alloy phase diagram.

εCo and 51.3vol.% αCo_2Si phases. The temperature interval between eutectic and eutectoid transformations is only 22K. Under equilibrium conditions, the eutectoid transformation occurs after the liquid/solid transformation. However, it may not be the case during rapid solidification.

3.1.Co-12.52%Si eutectic alloy

Under equilibrium solidification conditions, two eutectic phases nucleate competitively and grow cooperatively to form lamellar eutectic. However, the rapid solidification morphologies of Co-12.52%Si eutectic alloy display some different microstructures.

3.1.1. Rapid Solidification Microstructures

Figure 2 shows the rapid solidification microstructures of Co-12.52%Si eutectic alloy droplets with different sizes. From the experimental observations, it is found that most of the droplets consist of a mixture of lamellar eutectic and divorced eutectic grains. A large droplet with 600μm diameter is composed of lamellar eutectic grains completely. The enlarged view of a lamellar eutectic grain is presented in Fig. 2(a), in which the bright phase is εCo solid solution and the dark one is Co_3Si or αCo_2Si compound phase. The lamellar eutectic grain shows a feather-like morphology. With decreasing droplet size, the eutectic morphologies transform from lamellar eutectic to divorced eutectic. When the droplet diameter is smaller than 200μm, many droplets are composed entirely of divorced eutectic grains. Figure 2(b) presents an enlarged view of a small droplet with complete divorced eutectic. The two eutectic phases grow in a dendritic way to form divorced eutectic. It is necessary to identify whether the Si-rich phase is the same as that in large droplets. The EDS analysis shows that the Si-rich phase in small droplet involves roughly the same composition with that in the large droplet. In order to distinguish whether the dark phase is Co_3Si or αCo_2Si intermetallic compound, the XRD and EDS measurement results indicate that the dark phase in 600μm droplets is Co_3Si compound plus a little αCo_2Si, which cannot be identified from the other in Fig. 2. The XRD patterns of Fig. 3 indicate that the microstructures of undercooled Co-12.52%Si eutectic alloy are composed of εCo, αCo_2Si and Co_3Si phases. The metastable phase Co_3Si has resulted from the high undercooling condition. This displays that, with decreasing droplet size, the eutectoid reaction is restrained, and the Co_3Si compound cannot decompose completely in the undercooled alloy melt.

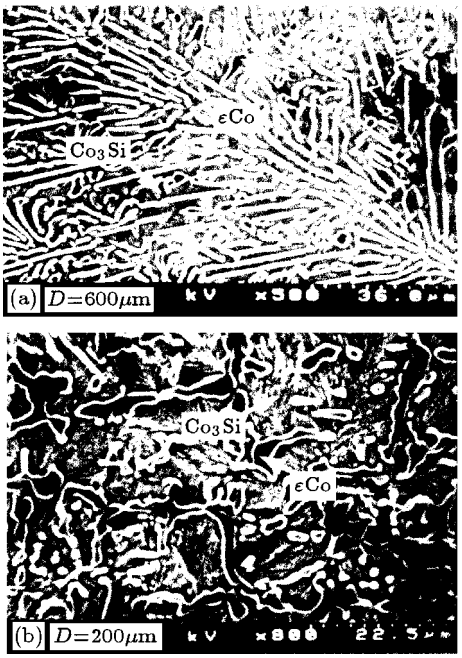


Fig.2. Rapid solidification microstructures of Co-12.52%Si eutectic alloy droplets with different sizes.

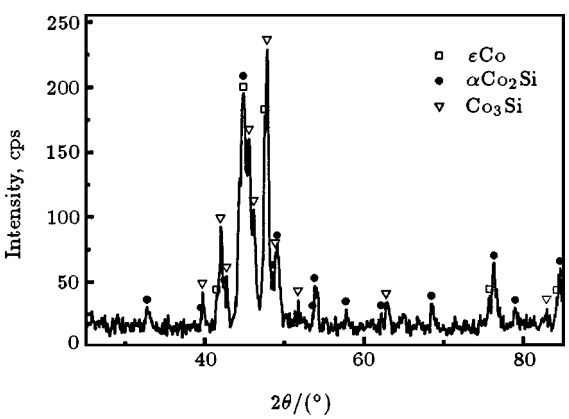


Fig.3. x-ray diffraction patterns of Co-12.52%Si eutectic alloy.

Based on the experimental observation and analysis, it is concluded that the microstructural evolution of Co-12.52%Si eutectic alloy has a transition from lamellar eutectic to divorced eutectic, as the droplet size reduces.

3.1.2. Cooling rate of droplets

During free fall, droplet size has a very important influence on the cooling rate (R_c). Because of such tiny droplets, measurement of cooling rate for every droplet is almost impossible. In an environment of inert gas, heat dissipation of droplets depends mainly on convection and radiation of the environment gas. Assuming the temperature gradient inside the droplet is very small, which can be ignored, the heat loss of

droplet during the free fall can be expressed by Eq.(1) based on the Newtonian model.

$$Q = Q_{\mathrm{r}} + Q_{\mathrm{c}} = A\varepsilon_{\mathrm{h}}\delta(T^4 - T_{\mathrm{out}}^4)t_{\mathrm{D}} + A(T - T_{\mathrm{out}})\int_0^{t_{\mathrm{D}}} h\mathrm{d}t. \quad (1)$$

Here, Q_{r} is the radiated heat loss, Q_{c} the heat loss of convection, A the surface area of the droplet, ε_{h} the radiation coefficient, δ the radiation constant, t_{D} the free fall time of the droplet, h the heat transfer coefficient. In the calculation, a superheat of 200K is used according to the detection of temperature of the bulk samples by an infrared pyrometer prior to dropping.

The average cooling rate of droplets can be obtained from the calculated heat loss of droplets.

$$R_{\mathrm{c}} = -\frac{\mathrm{d}T}{\mathrm{d}t} = \frac{1}{C_{\mathrm{p}}} \cdot \frac{\mathrm{d}Q}{\mathrm{d}t}. \quad (2)$$

Evidently, the average cooling rate increases drastically with decreasing droplet size, as seen in Fig. 4. For the droplets with diameters of 100 to 1000μm, R_{c} ranges from 2.1×10^4 to 4.4×10^1K/s.

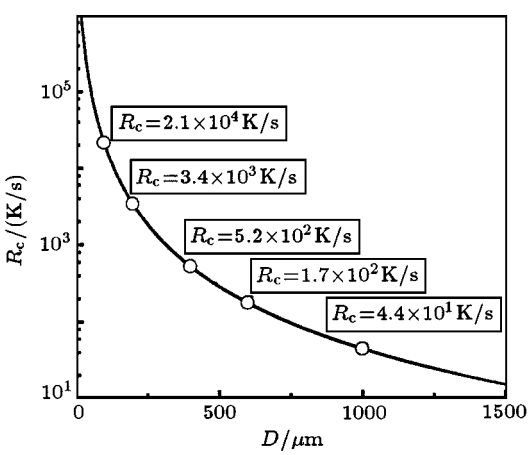


Fig.4. Calculated cooling rate of Co-12.52%Si eutectic alloy droplets versus droplet diameters.

3.1.3. Competitive nucleation characteristics

The nucleation rate of alloy melts can be described by the classical nucleation theory, which is expressed as[19]

$$I = I_0 \cdot \exp\left(-\frac{16\pi\sigma^3(T_{\mathrm{L}})^2}{3(\Delta H_{\mathrm{m}})^2(\Delta T)^2 kT} f(\theta)\right) \times \exp\left(-\frac{Q}{RT}\right), \quad (3)$$

where I_0 is the prefactor of nucleation, σ the interfacial energy which can be approximated by the interfacial model of Thompson and Spaepen,[20] R the gas constant; k is the Boltzmann constant, Q the activation energy for diffusion, T_{L} the liquidius temperature, θ the contact angle, $f(\theta)$ the catalytic factor, $f(\theta) = (2+\cos\theta)(1-\cos\theta)^2/4$.

Calculations indicate that no matter how large the undercooling is, the homogeneous nucleation rate will be far less than $1\mathrm{m}^{-3}\mathrm{s}^{-1}$, as illustrated in Fig. 5. This means that heterogeneous nucleation is more likely to take place. It can be deduced that the nucleation of εCo solid solution dominates the nucleation of droplets. The physical parameters used for calculations are listed in Table 1.

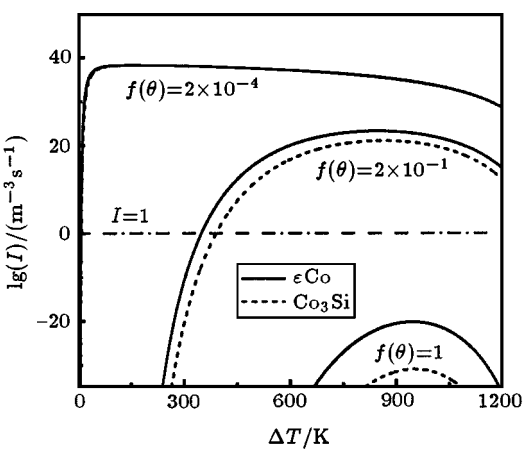


Fig.5. Calculated nucleation rates of Co-12.52%Si eutectic alloy.

For heterogeneous nucleation, the catalytic factor $f(\theta)$ should be determined. However, it is very difficult to obtain the data of contact angle. Evidently, at least one nucleus will solidify the whole sample, i.e.,

$$I \cdot v \cdot t \geq 1, \quad (4)$$

in which v is the volume of the droplet and t the solidification time. During our experiments, the volume of each droplet is calculated from its diameter. And the solidification time can be estimated from the cooling rate.

$$R_{\mathrm{c}} \cdot t = T_{\mathrm{i}} - T_{\mathrm{L}} + \Delta T, \quad (5)$$

where T_{i} is the temperature of droplet at the beginning of free fall, T_{L} the liquidius temperature. Based on Eqs.(3)–(5), the catalytic factor of droplets with different diameters can be estimated.

$$f(\theta) \leq -\frac{3(\Delta H_{\mathrm{m}})^2\Delta T^2 kT}{16\pi\sigma^3 T_{\mathrm{L}}^2} \times \left[\frac{Q}{RT} + \ln\frac{6R_{\mathrm{c}}}{\pi I_0(T_{\mathrm{i}} - T_{\mathrm{L}} + \Delta T)D^3}\right]. \quad (6)$$

It is known that, as the droplet diameter varies from 100 to 1000μm, the maximum of the catalytic factor

changes from 0.529 to 0.604. In other words, under the containerless conditions in drop tube, the homogeneous nucleation has no chance to take place for Co-12.52%Si eutectic alloy.

Table 1. Physical parameters of Co-Si alloys used for calculations.

Parameter	Symbol(unit)	Co-12%Si	Co-12.52%Si	Co-13%Si
Alloy composition	C_0/wt.%	12	12.52	13
Liquidus temperature	$T_{\rm L}$/K	1493	1477	1481
Heat of fusion	ΔH/(J/mol)	22141	22406	22648
Specific heat of liquid	$C_{\rm P}$/(J/mol·K)	33.5	33.5	33.4
Equilibrium liquidus slope	$m_{{\rm L}\varepsilon}$/(K/wt.%)	–36.0	–34.0	–30.8
Equilibrium liquidus slope	$m_{{\rm L}\alpha}$/(K/wt.%)	1.02	1.02	1.02
Pre-exponential term (diffusion)	D_0/(m^{2}s)	2.28×10^{-7}	2.28×10^{-7}	2.28×10^{-7}
Activation energy for diffusion	θ/(J/mol)	-6.58×10^{-10}	-6.58×10^{-10}	-6.58×10^{-10}
Characteristic length of diffusion	a_0/m	1.66×10^{-10}	1.70×10^{-10}	1.73×10^{-10}
Gibbs–Thomson coefficient	Γ_ε/Km	2.84×10^{-7}	2.85×10^{-7}	2.86×10^{-7}
Gibbs–Thomson coefficient	Γ_α/Km	2.82×10^{-7}	2.83×10^{-7}	2.84×10^{-7}
Sound velocity	V_0/(m/s)	3000	3000	3000
Solute partition coefficient	$k_{e\varepsilon}$	0.78	0.78	0.78
Solute partition coefficient	$k_{e\alpha}$	0.0	0.0	0.0
Interface energy of ε phase	$\sigma_{{\rm L}\varepsilon}$/(J/m^2)	0.595	0.595	0.594
Interface energy of α phase	$\sigma_{L\alpha}$/(J/m^2)	0.665	0.665	0.664

By assuming every phase has the same catalytic factor, the heterogeneous nucleation rates are illustrated in Fig. 5. It can be seen that, with increasing undercooling, the nucleation rates with rise at first and then reduce. Obviously, for Co-12.52%Si eutectic alloy, εCo solid solution is the primary nucleation phase under rapid solidification. The nucleation dominance of εCo solid solution becomes less with decreasing the catalytic factor. Overall, for Co-12.52%Si eutectic alloy, the homogeneous nucleation cannot occur when the droplets fall in drop tube. In heterogeneous nucleation, the primary nucleation phase is still εCo solid solution.

3.1.4. Estimation of droplet undercoolings

For free fall droplets, the undercooling cannot be measured accurately because of such small droplets. However, under containerless state, smaller droplet has fewer heterogeneous nuclei. This implies that smaller droplets can obtain higher undercooling. A heat transfer model[17] is used to estimate the nucleation temperature of droplet, from which the droplet undercooling can be deduced. The main principle of the model is as follows.

$$\frac{\Psi(D)}{T\cdot\Delta T^2}=\ln\Phi(T,D), \tag{7}$$

$$\Psi(D)=\frac{16\pi\sigma^3T_{\rm L}^2f(D)}{3k\rho_{\rm d}^2\Delta H^2}, \tag{8}$$

$$\Phi(T,D)=\frac{\frac{\pi}{6}D^3K_{\rm V}\Delta T^3T^2}{\Psi(D)\dot{T}(3T-T_{\rm L})+[\kappa+2\varepsilon(T-T_{\rm g})]\Delta T^3T^2}, \tag{9}$$

where $K_{\rm V}$ is the kinetic parameter taken here to have a value of $10^{40}{\rm m}^{-3}{\rm s}^{-1}$,[17] $T_{\rm g}$ the gas temperature in the drop tube, $\rho_{\rm d}$ the density of the melt, $f(D)$ the contact angle factor. Assuming an inverse relationship between catalytic efficiency and the droplet diameter[18] with typical values of $f(\theta)$=1.0×10^{-4} for 1000μm droplets and $f(\theta)$=4.5×10^{-2} (which is the maximum of the catalytic factor obtained from Eq.(6).) for 10μm droplets, the following equation can be obtained.

$$f(\theta)=\frac{1}{4}(2-3\cos\theta+\cos^3\theta)=a+\frac{b}{D}, \tag{10}$$

with a=–0.004 and b=4.574μm. The functions of κ and ε can be obtained by Ref. [17]. Based on the nucleation temperature of droplets with different diameters, the undercooling versus droplet diameter is presented in Fig. 6. Evidently, with decreasing droplet diameter, the droplet undercooling increases rapidly. There exists a relationship between them as follows:

$$\Delta T=24.5+271{\rm e}^{-0.004D}. \tag{11}$$

Corresponding to the droplets of 600μm and 200μm, which are shown in Fig. 2, the undercoolings are

51K and 131K, respectively. Therefore, with the enhancement of undercooling, the rapidly solidified microstructures have a transition from lamellar eutectic to divorced eutectic.

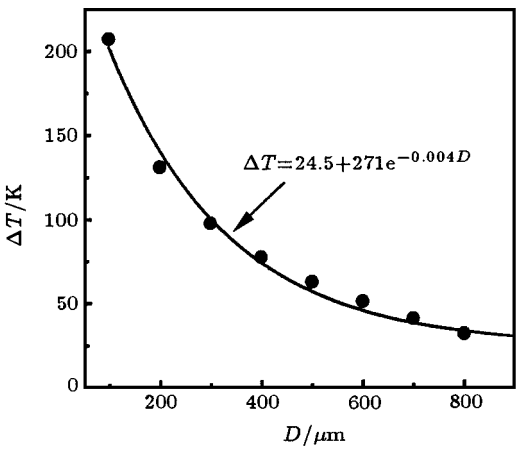


Fig.6. Droplet undercooling versus droplet diameter.

3.1.5. Dendritic and eutectic growth kinetics

Based on the experimental results, it can be observed that the microstructural evolution of Co-12.52%Si eutectic alloy transforms from lamellar eutectic to divorced eutectic with increasing undercooling. To understand the growth mechanism, the rapid dendritic (LKT)[21] and eutectic (TMK)[22] growth models have been used to calculate the growth velocities of dendrites and lamellar eutectic.

According to LKT dendritic growth model, the interrelationship between growth velocity V, dendrite tip radius R, and undercooling ΔT is uniquely determined by the following two coupled equations when taking into account the BCT analysis of nonequilibrium interface kinetics.

$$\Delta T = \Delta T_{\rm t} + \Delta T_{\rm c} + \Delta T_{\rm r} + \Delta T_{\rm k}, \tag{12}$$

$$R = \frac{\Gamma/\sigma^*}{P_{\rm t}\xi_{\rm t}\dfrac{\Delta H}{C_{\rm P}} - \dfrac{2m'_{\rm L}C_0(1-k_{\rm V})P_{\rm c}}{1-(1-k_{\rm V})I_{\rm V}(P_{\rm c})}\xi_{\rm c}}, \tag{13}$$

where $\Delta T_{\rm t}$ represents the thermal undercooling, $\Delta T_{\rm c}$ the solute undercooling, $\Delta T_{\rm r}$ the curvature undercooling, and $\Delta T_{\rm k}$ the kinetic undercooling. Γ is the Gibbs–Thomson coefficient, $P_{\rm t}$ the thermal Peclet number, $P_{\rm c}$ the solute Peclet number, $I_{\rm V}(P_{\rm c}) = P_{\rm c}\exp(P_{\rm c})E_{\rm I}(P_{\rm c})$ the Ivantsov function of solute Peclet number, σ^* the stability constant, $m'_{\rm L}$ the actual liquidius slope under nonequilibrium conditions, $\xi_{\rm c}$ the solute stability function, and $\xi_{\rm t}$ the thermal stability function. $k_{\rm V}$ is the actual solute partition coefficient, which is derived from Ref. [21].

TMK eutectic growth model describes the ΔT-V-λ (undercooling, eutectic growth velocity, interlamellar spacing) interrelationship by the following two equations after considering the influence of nonequilibrium interface kinetics.

$$\lambda^2 V = a_{\rm L}/Q_{\rm L}, \tag{14}$$

$$\lambda\Delta T = ma_{\rm L}\left[1 + \frac{P}{P + \lambda(\partial P/\partial\lambda)}\right]. \tag{15}$$

Here P is a function of solutal Peclet number for eutectic growth and actual partition coefficient ($k_{\rm V}$). $a_{\rm L}$ is a function of capilarity constants, equilibrium liquidius slopes, partition coefficients and the volume fractions (f) of the two eutectic phases. $Q_{\rm L}$ is a function of λ, f, P and diffusion coefficient.

The calculated growth velocities of dendrites and lamellar eutectic in Co-12.52%Si eutectic alloy have been shown in Fig. 7. Physical parameters used in calculations are listed in Table 1. Figure 8 illustrates that, when undercooling becomes larger, the growth velocity of lamellar eutectic in Co-12.52%Si eutectic alloy increases rapidly and then reduces to zero at ΔT=4.8K. It shows that lamellar eutectic cannot form when undercooling is larger than 4.8K. The growth of Co_3Si dendrite will be dominant under undercoolings higher than 4.8K. Because the eutectoid transformation occurs at 22K below the eutectic line, it can be deduced that Co_3Si compound formed in the lamellar eutectic will decompose into εCo and αCo_2Si phases. However, in an undercooled alloy melt, the decomposition of Co_3Si compound is restrained. As the undercooling is higher than 22K, Co_3Si compound formed in the divorced eutectic grows from the undercooled alloy melt and cannot decompose completely into εCo and αCo_2Si phases.

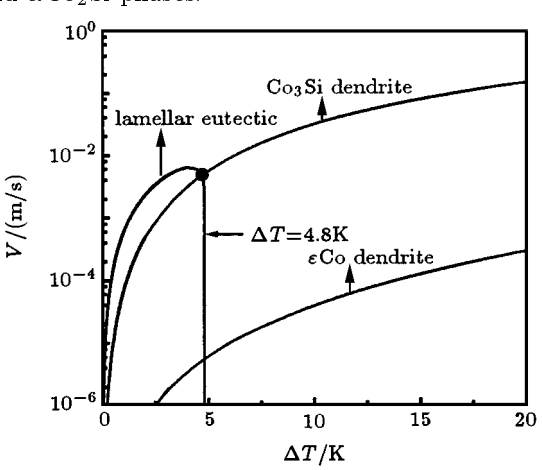


Fig.7. Calculated growth velocities of dendrites and lamellar eutectic in Co-12.52%Si eutectic alloy.

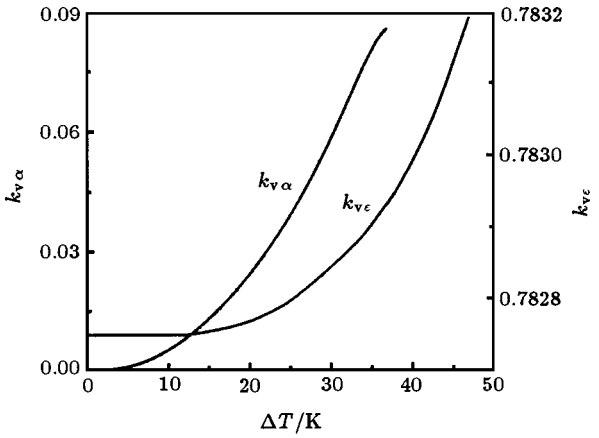


Fig.8. Calculated actual solute partition coefficients of εCo and Co_3Si phases in Co-12.52%Si eutectic alloy.

Figure 8 illustrates the actual solute partition coefficients of the εCo solid solution ($k_{v\varepsilon}$) and Co_3Si compound ($k_{v\alpha}$) under different undercoolings. Obviously, when the undercooling increases, both of the actual solute partition coefficients increase. The increment per unit undercooling of Co_3Si compound ($dk_{v\alpha}/d\Delta T$) is always larger than that of εCo solid solution ($dk_{v\varepsilon}/d\Delta T$), i.e.

$$\frac{dk_{v\alpha}}{d\Delta T} > \frac{dk_{v\varepsilon}}{d\Delta T}. \tag{16}$$

In other words, high undercooling can suppress the microsegregation in the binary alloy. The reduction rate in Co_3Si compound is larger than that in εCo solid solution.

3.1.6. Eutectic coupled zone

The competitive growth theories of dendrites and lamellar eutectic establish the idea of eutectic coupled zone, which has been calculated around Co-12.52%Si eutectic alloy and shown also in Fig. 1. It can be seen that the eutectic coupled zone leans to the Co-rich side and covers a composition range from 11.6 to 12.7%Si. An undercooling of 0–5K will result in a complete lamellar eutectic microstructure for Co-12.52%Si eutectic alloy. In the experiment, it is found that, for Co-12.52%Si eutectic alloy, most of the droplets consist of a mixture of lamellar eutectic and divorced eutectic grains. In other words, divorced eutectic grain forms very easily in droplets. Evidently, for Co-12.52%Si eutectic alloy droplets, the critical undercooling of eutectic coupled zone is easy to reach during free fall. Judging from the eutectic coupled zone, it can be predicted that off-eutectic alloy, the composition of which ranges from 11.6 to 12.7%Si, can form a eutectic microstructure when the undercooling is higher than a certain value.

3.2.Co-12%Si and Co-13%Si off-eutectic alloys

3.2.1. Microstructural evolution of Co-12%Si hypoeutectic alloy

Figure 9 shows the microstructure morphologies of Co-12%Si hypoeutectic alloy droplets with different sizes. Based on the experimental observation, with decreasing droplet size, the morphologies show a reduction of volume fraction of the primary εCo phase, and the microstructural evolution experiences a transition from εCo dendrite plus lamellar eutectic to anomalous eutectic. Figure 9(a) is an enlarged view of a large droplet with a diameter of 1000μm, in which the lamellar eutectic forms in the interdendritic spacing of primary εCo. When the droplet diameter becomes smaller, the primary εCo phase transforms from dendrite to equiaxed grain and the volume fraction of primary εCo phase reduces evidently. Figure 9(b) shows an enlarged part of a small droplet with a diameter of 200μm, which consists of anomalous eutectic. Clearly, the morphologies display a chrysanthemum-like anomalous eutectic. The experimental observation for Co-12%Si hypoeutectic alloy indicates that the microstructure is characterized by the primary εCo phase plus eutectic. With increasing undercooling, the microstructural evolution of Co-13%Si alloy transforms from εCo dendrite plus lamellar eutectic to anomalous eutectic. For understanding the microstructural evolution, the grain size of primary εCo phase is measured.

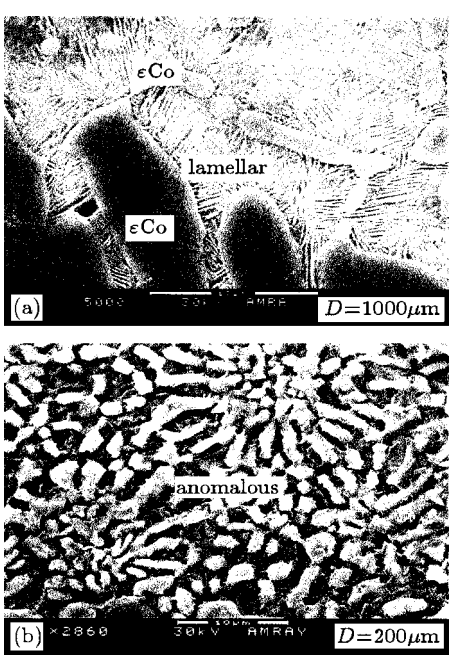


Fig.9. Rapid solidification microstructures of Co-12%Si hypoeutectic alloy droplets with different sizes.

Fig. 10 presents the relationship between the average grain size (d_g) of primary εCo phase and the droplet undercooling (ΔT). The primary εCo phase is refined with the enhancement of undercooling. Based on the experimental measurements, the relationship between ΔT and d_g is established as

$$d_g = 2.02 \times 10^3 \Delta T^{-0.75}. \quad (17)$$

Therefore, the average grain size (d_g) of primary εCo phase decreases rapidly when the undercooling becomes greater.

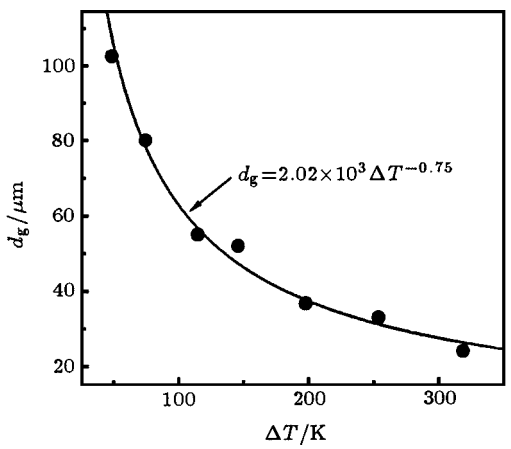


Fig.10. Average grain size of primary εCo phase versus droplet undercooling.

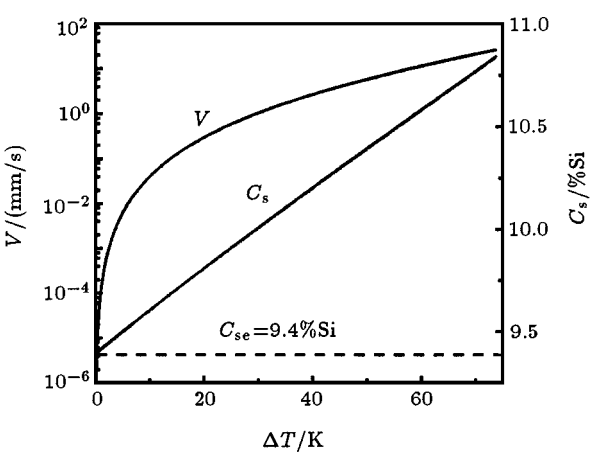


Fig.11. Calculated growth velocity and interfacial solid composition of εCo versus undercooling.

The calculated nucleation rates of εCo and Co_3Si phases in the Co-12%Si hypoeutectic alloy indicate that homogeneous nucleation cannot occur during rapid solidification, and the primary nucleation phase is εCo solid solution. The growth velocity of primary εCo phase has been calculated using LKT[21] dendritic growth theory, as Fig. 11 illustrates. With increasing undercooling, the growth velocity of εCo phase rises steeply. Furthermore, the interfacial solid composition (C_s) of εCo phase versus undercooling is also shown in Fig. 11. When the undercooling is not very large, the interfacial solid composition of εCo increases linearly from the equilibrium solid composition C_{se}=9.4%Si with the enhancement of undercooling.

The bulk undercooling is the sum of partial undercoolings including the thermal undercooling (ΔT_t), the solutal undercooling (ΔT_c), the curvature undercooling (ΔT_r), and the kinetic undercooling (ΔT_k). Figure 12 shows the contributions of partial undercoolings to the bulk undercooling of εCo phase. As the bulk undercooling increases, partial undercoolings all become large. The solutal undercooling is the main contribution to the bulk undercooling. The growth of εCo phase in undercooled alloy melt is controlled by the solutal diffusion. The thermal diffusion cannot replace the solutal diffusion to control the growth of εCo phase.

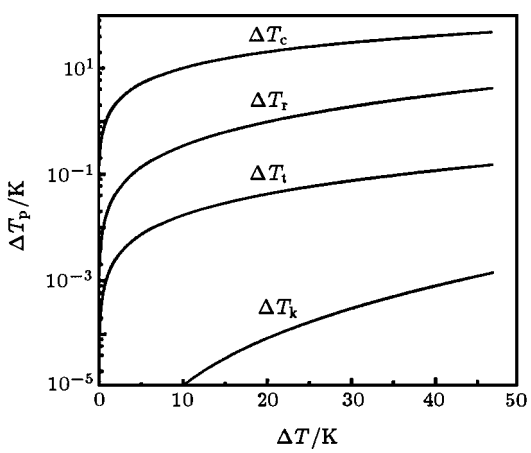


Fig.12. Contributions of partial undercoolings to bulk undercooling for εCo phase in Co-12%Si hypoeutectic alloy.

The selected composition of Co-12%Si hypoeutectic alloy is in the composition range of eutectic coupled zone. The experimental result shows that, as undercooling increases, the primary εCo phase is refined and the chrysanthemum-like anomalous eutectic formed in the small droplets. To investigate the competitive growth between the primary phase and eutectic microstructure, a Co-13%Si hypereutectic alloy is selected to be rapidly solidified in drop tube by containerless processing.

3.2.2. Microstructural evolution of Co-13%Si hyper eutectic alloy

Figure 13 illustrates the rapidly solidified microstructures of droplets with different sizes. Appar-

ently, with decreasing droplet size, i.e., with increasing undercooling, the morphologies undergo a transition from dendrite to equiaxed grain. Figure 13(a) displays an enlarged part of a droplet with a diameter of 1000μm, in which the primary dendrites have many remelted traces. Eutectic microstructure forms in the spacing between remelted dendrites. The EDS analysis indicates that the primary dendrite is Co_3Si compound, which cannot decompose completely into εCo and αCo_2Si phases. When undercooling becomes larger, equiaxed grains can form in droplets, as shown in Fig. 13(b). The primary Co_3Si compound grew homogeneously in the undercooled alloy melt to form equiaxed grains. From the observations of morphologies, the volume fraction of the primary phase does not change evidently. And the morphologies in the interdendritic spacing are eutectic microstructures, no matter how small the droplet diameter is. On the basis of experimental analysis, it can be concluded that the rapidly solidified microstructure of the Co-13%Si hypereutectic alloy is characterized by primary Co_3Si compound plus eutectic microstructures, and with the enhancement of undercooling, the primary Co_3Si phase transforms from dendrites to equiaxed grains.

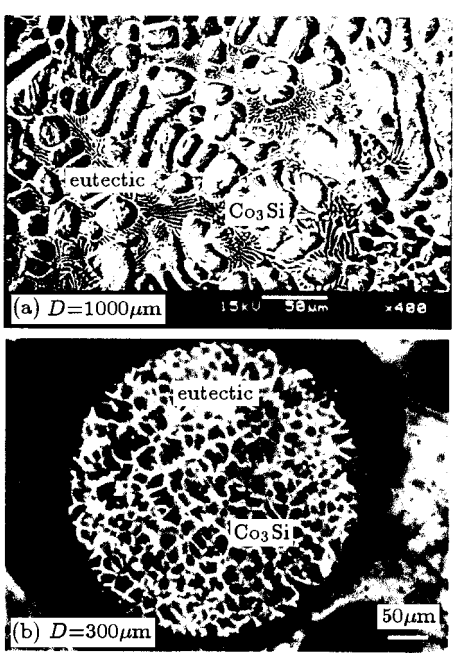


Fig.13. Rapid solidification microstructures of Co-13%Si hypereutectic alloy droplets with different sizes.

The measurement of the primary Co_3Si grain size has been done to establish the relationship between the average grain size of primary Co_3Si phase and droplet undercooling. Figure 14 is the measured result. The fitted line illustrates that the primary Co_3Si phase is refined, when undercooling increases. The relationship between the average grain size (d_g) of the primary Co_3Si phase and the droplet undercooling (ΔT) is shown as follows:

$$d_g = 3.61 \times 10^2 \Delta T^{-0.52}. \quad (18)$$

Evidently, the average grain size of the primary Co_3Si phase decreases dramatically with increasing undercooling.

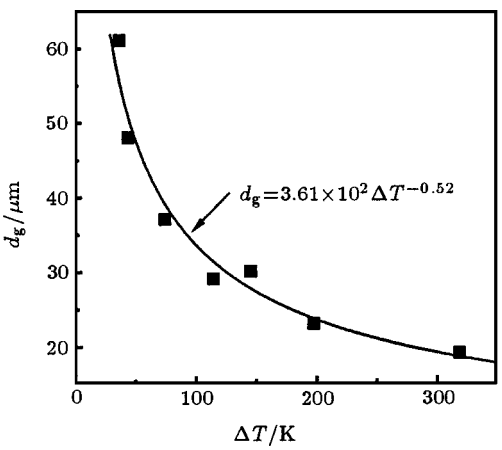


Fig.14. Average grain size of primary Co_3Si phase versus droplet undercooling.

The calculated results for the competitive nucleation and growth of εCo and Co_3Si phases indicate that, homogeneous nucleation cannot be realized in an undercooled Co-13%Si melt. εCo solid solution is the primary nucleation phase but not the primary growth phase for Co-13%Si alloy. Figure 15 shows the calculated growth velocity of primary Co_3Si phase. It can be seen that the growth velocity of primary Co_3Si phase rapidly becomes bigger with the enhancement of undercooling. Under the same undercooling, the growth velocity of primary Co_3Si phase in Co-13%Si hypereutectic alloy is much higher than the growth velocity of primary εCo phase in Co-12%Si hypoeutectic alloy. Additionally, the composition of Co-13%Si hypereutectic alloy exceeds the composition range of eutectic coupled zone. The analysis explains that, with the enhancement of undercooling, the primary Co_3Si phase in the Co-13%Si hypereutectic alloy transforms from dendrites to equiaxed grains. The interfacial solid composition (C_s) of the primary Co_3Si phase in Co-13%Si hypereutectic alloy is also illustrated in Fig. 15. As undercooling goes up, the interfacial solid composition of the primary Co_3Si phase decreases from C_s=13.8%Si towards the melt composition 13%Si.

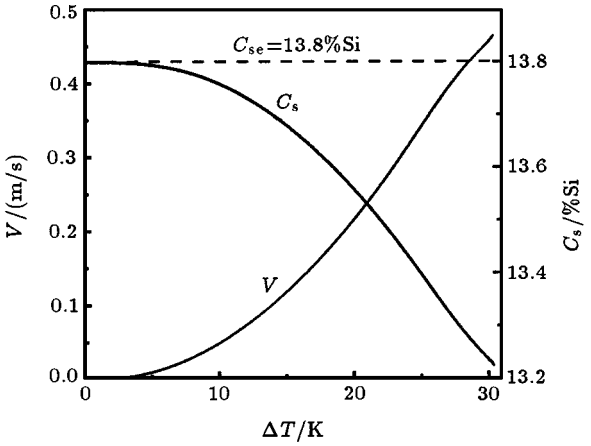


Fig.15. Calculated growth velocity and interfacial solid composition of the primary Co_3Si phase in Co-13%Si hypereutectic alloy versus undercooling.

Figure 16 presents the contributions of partial undercoolings for the primary Co_3Si phase in Co-13%Si hypereutectic alloy to the bulk undercooling. Except that the curvature undercooling increases at first and then decreases, all of the partial undercoolings become larger with the enhancement of bulk undercooling. From Fig. 16, it is obvious that the solutal undercooling is the main contribution to the bulk undercooling. Consequently, the growth of primary Co_3Si phase in the Co-13%Si hypereutectic alloy is controlled by the solutal diffusion.

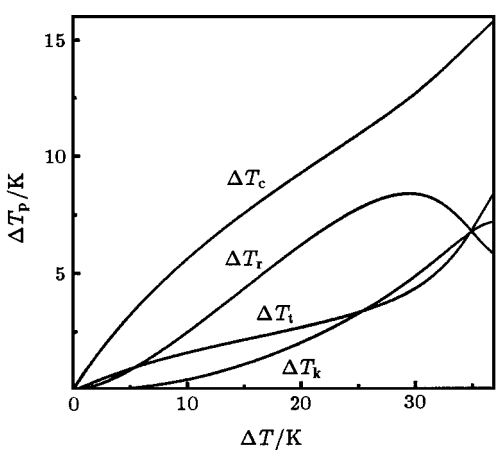


Fig.16. Calculated partial undercoolings of primary Co_3Si phase in Co-13%Si hypereutectic alloy versus bulk undercooling.

4. Conclusions

The containerless rapid solidification of Co-12.52%Si eutectic alloy has been realized in drop tube. The rapidly solidified microstructures are characterized by (εCo+Co_3Si) eutectic. When the undercooling increases, the structural morphologies of Co-12.52%Si eutectic alloy transform from lamellar eutectic to divorced eutectic. The EDS and XRD analyses reveal that the Co_3Si compound cannot decompose completely in the undercooled alloy melt. Calculations indicate that the lamellar eutectic of εCo and Co_3Si forms only if the undercooling is smaller than 4.8K.

The calculated nucleation rates of εCo solid solution and Co_3Si compound in the Co-Si system show that homogeneous nucleation cannot occur in undercooled alloy melts, and the εCo solid solution is the primary nucleation phase. The eutectic coupled zone around Co-12.52%Si eutectic alloy is calculated on the basis of competitive growth principle. The composition range of the eutectic coupled zone is from 11.6 to 12.7%Si. And the temperature range is very small.

The rapidly solidified microstructures of Co-12%Si hypoeutectic alloy, the composition of which is in the composition range of eutectic coupled zone, consist of the primary εCo phase plus eutectic microstructure. With the enhancement of undercooling, the primary εCo phase is refined. Experimental observations indicate that the volume fraction of the primary εCo phase decreases significantly, as droplet undercooling increases. Furthermore, the eutectic microstructure formed in the interdendritic spacing displays a transition from lamellar eutectic to chrysanthemum-like anomalous eutectic, when the undercooling rises. Calculated results demonstrate that the growth of primary εCo phase is controlled by the solutal diffusion, no matter how large the undercooling is.

For Co-13%Si hypereutectic alloy, the composition of which is out of the composition range of eutectic coupled zone, the rapid solidification microstructure is composed of primary Co_3Si compound and lamellar eutectic. When undercooling becomes greater, the primary Co_3Si phase transforms from dendrite to equiaxed grains. Theoretical analysis indicates that, with the enhancement of undercooling, the growth of primary Co_3Si phase is controlled by the solutal diffusion.

Acknowledgement

The authors are grateful to Professor C. D. Cao, Dr. N. Wang, Dr. W. J. Xie and Mr. Y. J. Lü for their stimulating discussions and help during experiments.

References

[1] Su R *et al* 2002 *Acta Phys. Sin.* **51** 2325
[2] Cao C D *et al* 2000 *Sci. Chin.* A **24** 1318
[3] Lee Y P *et al* 1999 *Phys. Rev.* B **60** 8067
[4] Kim S K *et al* 2000 *Phys. Rev.* B **62** 3025
[5] Baker H 1992 *ASM Handbook vol. 3 Alloy Phase Diagrams* 1st edn (Ohio: The Materials Information Society) p2148
[6] Detavernier C *et al* 2001 *J. Appl. Phys.* **89** 2146
[7] Qu X P *et al* 2001 *J. Appl. Phys.* **89** 2641
[8] Detavernier C *et al* 2000 *Phys. Rev.* B **62** 12045
[9] Yao W J *et al* 2002 *Mater. Sci. Eng.* A **344A** 10
[10] Tournier S *et al* 1998 *Phys. Rev.* B **57** 3340
[11] Cortella L *et al* 1993 *Phys. Rev. Lett.* **70** 1469
[12] Yao W J *et al* 2003 *Acta Phys. Sin.* **52** 448
[13] Fransaer J *et al* 2000 *J. Appl. Phys.* **87** 1801
[14] Lacy L L *et al* 1981 *J. Crys. Growth.* **51** 47
[15] Yao W J *et al* 2002 *Chin. Sci. Bull.* **47** 1316
[16] Yu R C *et al* 1996 *Acta Phys. Sin.* **45** 628
[17] Lee E S *et al* 1994 *Acta Metall Mater* **42** 3231
[18] Grant P S *et al* 1993 *Acta Metall Mater* **41** 3097
[19] Kurz W and Fisher D J 1989 *Fundamentals of Solidification* 3rd edn (Amsterdam: Trans Tech) p28
[20] Thompson C V *et al* 1983 *Acta Metall Mater* **31** 2021
[21] Lipton J *et al* 1987 *Acta Metall Mater* **35** 957
[22] Trivedi R *et al* 1987 *Acta Metall Mater* **35** 971